5-22-2020

The Planetary Luminosity Problem: " Missing Planets" and the Observational Consequences of Episodi Accretion

Sean D. Brittain
Clemson University, sbritt@clemson.edu

Joan R. Najita
National Optical Astronomical Observatory

Ruobing Dong
University of Victoria

Zhaohuan Zhu
University of Nevada, Las Vegas, zhaohuan.zhu@unlv.edu

Follow this and additional works at: https://digitalscholarship.unlv.edu/physastr_fac_articles

Part of the External Galaxies Commons, Instrumentation Commons, and the Stars, Interstellar Medium and the Galaxy Commons

Repository Citation

The Planetary Luminosity Problem: "Missing Planets" and the Observational Consequences of Episodic Accretion

Sean D. Brittain[1,5] , Joan R. Najita[2] , Ruobing Dong[3] , and Zhaohuan Zhu[4]
[1] Clemson University, 118 Kinard Laboratory, Clemson, SC 29634, USA; sbritt@clemson.edu
[2] National Optical Astronomical Observatory, 950 North Cherry Avenue, Tucson, AZ 85719, USA
[3] Department of Physics & Astronomy, University of Victoria, Victoria, BC V8P 1A1, Canada
[4] Department of Physics and Astronomy, University of Nevada, Las Vegas, 4505 South Maryland Parkway, Las Vegas, NV 89154, USA

Abstract

The high occurrence rates of spiral arms and large central clearings in protoplanetary disks, if interpreted as signposts of giant planets, indicate that gas giants commonly form as companions to young stars ($<$few Myr) at orbital separations of 10–300 au. However, attempts to directly image this giant planet population as companions to more mature stars ($>$10 Myr) have yielded few successes. This discrepancy could be explained if most giant planets form by "cold start," i.e., by radiating away much of their formation energy as they assemble their mass, rendering them faint enough to elude detection at later times. In that case, giant planets should be bright at early times, during their accretion phase, and yet forming planets are detected only rarely through direct imaging techniques. Here we explore the possibility that the low detection rate of accreting planets is the result of episodic accretion through a circumplanetary disk. We also explore the possibility that the companion orbiting the Herbig Ae star HD 142527 may be a giant planet undergoing such an accretion outburst.

Unified Astronomy Thesaurus concepts: Herbig Ae/Be stars (723); Circumstellar disks (235); Planet formation (1241); Protoplanetary disks (1300); Exoplanet detection methods (489); Exoplanet astronomy (486)

1. Introduction

Giant planets are common at small orbital separations, as are indirect signatures of their existence at large separations. At orbital separations $\lesssim$10 au, 10%–20% of low-mass stars (LMSs; $<$1.5 $M_\odot$) host a gas giant planet ($\gtrsim$1 M_J; Cumming et al. 2008; Cassan et al. 2012). At large separations ($\gtrsim$10 au), a high occurrence rate of giant planetary companions to LMSs is also inferred, based on the morphologies of protoplanetary disks surrounding young LMSs (i.e., T Tauri stars). Some 10%–15% of T Tauri disks have the spectral energy distribution (SED) of a transition disk, i.e., a protoplanetary disk in which the central portion ($\lesssim$10–40 au) is optically thin in the IR continuum (Muzerolle et al. 2010). Transition disk morphologies and other corroborating properties are interpreted as the signpost of one or more giant planets ($\gtrsim$3 M_J) orbiting within the optically thin region of the disk (Dodson-Robinson & Salyk 2011; Zhu et al. 2011; Espaillat et al. 2014).

A similar story is found for giant planet companions to intermediate-mass stars (IMSs; $\sim$1.5–2 $M_\odot$). At small orbital separations, radial velocity studies find that $\sim$14% of IMSs harbor a gas giant planet within $\sim$10 au of the star (Johnson et al. 2010; Luhn et al. 2019). Transition disk SEDs are also common among young IMSs (i.e., Herbig Ae stars); approximately 40% of Herbig Ae stars within 200 pc are transition disk sources (S. D. Brittain & J. R. Najita 2020, in preparation). In addition, a surprisingly large fraction of well-studied Herbig Ae disks show dramatic two-arm spirals ($\sim$20%; Dong et al. 2018b), which point to the presence of high-mass giant planets ($5–13 M_J$) at 30–300 au (Fung & Dong 2015; Dong & Fung 2017).

In contrast to the high frequency of indirect indicators of giant planets beyond $\sim$10 au, direct detection of the planets

themselves has proven challenging as companions to both mature stars and young stars surrounded by protoplanetary disks. Many high-contrast imaging surveys have searched for giant planet companions to stars older than 10 Myr at orbital separations $>$10 au. As summarized by Bowler (2016; see also Nielsen et al. 2019), such studies find that high-mass planets ($5–13 M_J$) are detected at 30–300 au orbital separation in only a small fraction of mature IMSs (2.8%; Bowler 2016), assuming they are as bright as predicted by "hot start" planetary evolutionary models. The low incidence rate is much less than the $\sim$20% two-arm spiral arm fraction of young IMSs that points to planets in the same range of mass and orbital separation (Dong et al. 2018b). For mature LMSs, $\sim$1% have a 1–13 M_J giant planet at 10–100 au (Figure 18 of Nielsen et al. 2019), a much lower occurrence rate than the 10%–15% occurrence rate of transition disks among the T Tauri star population.

The discrepancy between the detection rates of indirect signposts of planet formation and of the planets themselves could indicate that the indirect signposts are caused by something other than planets. For example, two-armed spirals can also arise from gravitationally unstable disks (Dong et al. 2015a; Kratter & Lodato 2016). However, the lifetime of the gravitationally unstable phase is too short to account for the large number of two-armed spirals observed around young stars (Dong et al. 2018b; Hall et al. 2018).

Alternatively, the discrepantly low detection rate of high-mass giant planets as companions to mature stars could be entirely due to the use of the hot start models, which assume that planets retain their heat of formation (i.e., gravitational potential energy) when they form. The alternative "cold start" models (Marley et al. 2007; Fortney et al. 2008) assume that planets radiate away much of their accretion energy in the formation phase. As a result, they predict considerably fainter planets at ages $>$10 Myr compared to hot start models.

---

[5] Visiting Scientist, NOAO.

Stone et al. (2018) found that essentially all nearby FGK stars could harbor one or more 7–10 M_J planets at 5–50 au if they formed by cold start. The planets are simply too faint to be detected with current surveys.

While the above discrepancy could point to the validity of cold start models over hot start models, that scenario implies that accreting planets would be very bright in their youth as they radiate away their accretion energy in accretion shocks and/or through a circumplanetary disk. That is, young giant planets (<few Myr) embedded in protoplanetary disks should be readily detectable during their runaway accretion phase (Eisner 2015; Zhu 2015).

So it is perhaps surprising that giant planets are detected infrequently as companions to young stars surrounded by protoplanetary disks. While transition disks have been targeted in many high-contrast imaging studies (e.g., Subaru SEEDS), planetary companion candidates have been detected in only a few sources. The best candidates to date are the companions to two LMS transition disks—PDS 70 (Keppler et al. 2018) and LkCa 15 (Kraus & Ireland 2012; Sallum et al. 2015)—and the companions to the IMS transition disk HD 100546 (Brittain et al. 2019; Pérez et al. 2019). As in the case of the spatially resolved (stellar) companion to the IMS transition disk HD 142527 (Biller et al. 2012; Close et al. 2014), Hα emission from the PDS 70 and LkCa 15 companions suggests that they are actively accreting.

Here we explore the reason for the infrequent detection of accreting giant planets in protoplanetary disks despite the likelihood that such planets occur commonly and radiate away their accretion energy as they accrete. We propose that the low "luminosity problem" of forming planets is solved in a similar fashion to the luminosity problem of forming stars (Kenyon et al. 1990; Kenyon & Hartmann 1995). Namely, forming planets accrete episodically in a similar way to forming stars undergoing FU Ori–like outbursts. Previous studies have argued that circumplanetary disks, like circumstellar disks, are likely to harbor significant dead zones and would accrete episodically (Lubow & Martin 2012), or that vortices form in circumplanetary disks and generate short-timescale outbursts (Zhu et al. 2016).

To explore this scenario in the context of the developing detection statistics and properties of young planetary companions, we summarize in Section 2 the properties of resolved planetary companions to young protoplanetary disk sources. In Section 3, we describe a simple toy model for episodic accretion based on the theoretical literature and illustrate how episodic accretion can potentially account for the low detection rate of accreting planets. In Section 4, we explore the possibility that the companion to HD 142527 is actually a planetary companion undergoing an accretion outburst rather than a low-mass stellar companion and discuss ways to discriminate between the two possibilities.

2. Searches for Young Planets

The largest published near-IR (NIR) imaging survey for planets forming in protoplanetary disks was carried out in the SEEDS campaign using Subaru/HiCIAO. Uyama et al. (2017) reported SEEDS observations of 68 young stellar objects (39 LMSs and 29 IMSs) at NIR wavelengths. Some of the targets were primarily observed in polarization differential imaging mode to probe disk structures, while a fraction of the targets were observed in angular differential imaging (ADI) mode under decent conditions. Specifically, for 20 targets, a 5σ contrast level of 5 mag or more was achieved at the H band at

0″25 separation, which corresponds to a typical upper limit on a planet's H-band luminosity of 3×10^{31} erg s^{-1} μm^{-1} (Table 1) and a planet mass limit of 5–10 M_J at a few tens of au, assuming hot start models (Baraffe et al. 2003). These results are based on conventional ADI data reduction and have not taken into account the effects of circumplanetary material on the detectability of embedded planets (Maire et al. 2017).

Other searches using ADI, carried out for planets forming in individual protoplanetary disks, have probed smaller orbital separations ~0″1 and lower companion luminosities (e.g., Cieza et al. 2013; Quanz et al. 2013; Currie et al. 2015, 2017; Testi et al. 2015; Canovas et al. 2017; Follette et al. 2017; Maire et al. 2017; Guidi et al. 2018; Keppler et al. 2018; Ligi et al. 2018; Reggiani et al. 2018; Sissa et al. 2018; Cugno et al. 2019; Gratton et al. 2019). Similarly, aperture masking has been used to probe even smaller separations (e.g., Biller et al. 2012; Kraus & Ireland 2012; Grady et al. 2013; Kraus et al. 2013; Sallum et al. 2015; Willson et al. 2016). The results of these observations are summarized in Table 1.

In addition to NIR searches for forming planets in disks, there have been several efforts to image Hα emission arising from the accretion shock on the forming planet. Several studies have targeted individual objects (HD 142527, Close et al. 2014; LkCa 15, Sallum et al. 2015; PDS 70, Haffert et al. 2019, Wagner et al. 2018). In a recent study, Zurlo et al. (2020) studied 11 nearby transition disks with SPHERE on the Very Large Telescope and found no Hα emission from accreting planets down to an upper limit on accretion luminosity of 10^{-6} $L_\odot$ at 0″2, which is about 3 orders of magnitude below the accretion luminosity inferred for LkCa 15b (Sallum et al. 2015).

Table 1 lists the 40 sources from the SEEDS study and the studies of individual disks that have been observed with ADI or aperture masking. Of these, 24 are LMSs and 16 are IMSs (column 2). Of the 40 sources, 20 have been classified as transition disks (column 4). The four sources with two-arm spirals—the other signature of high-mass giant planets—are all transition disk sources. Column 5 provides the cavity size of the transition disks. Columns 6 and 7 list the inner and outer extent of the region of the disk that has been imaged. Columns 8–10 present the NIR magnitude of the stars, columns 11–13 present the contrast limits achieved at 0″25, and columns 14–16 present the corresponding measured value or upper limit on λL_λ of a companion in each band. Assuming the colors of an accreting disk source (see Section 3), these upper limits are sufficient to detect a companion as bright as $0.1 L_\odot$ and sometimes much fainter.

The above studies have tended to focus on disks with spiral arms, gaps, and cavities, which are potential signposts of planets (e.g., Dong et al. 2015b, 2015c). Unlike direct imaging searches for planets around stars without a disk, searches for planets in disk-bearing systems are complicated by the effect of the protoplanetary disk material on the detectability of embedded planets (e.g., Maire et al. 2017). As shown in the table, most such efforts have yielded nondetections. For example, Maire et al. (2017) and Canovas et al. (2017) reported the nondetection of planets in the SAO 206462 and 2MASS J1604 disks, respectively, and placed an upper limit of a few Jupiter masses on the mass of putative planets at $r \gtrsim 100$ au in the former and $r \gtrsim 30$ au in the latter.

Among these 40 systems, the most secure detection of accreting protoplanets is in PDS 70 (Keppler et al. 2018; Haffert et al. 2019). This object has detected companions at

Table 1
Stars with Protoplanetary Disks Imaged within 0″.25 with Sufficient Sensitivity to Detect a 0.1 $L_\odot$ Companion

Star	Type	Distance	Morphology[a]	Cavity Size	Inner Extent	Outer Extent	Stellar Magnitude			Contrast			λL_λ		
		(pc)		(au)	(au)	(au)				(10^{-3} Magnitudes)			(10^{30} erg s^{-1})		
							H	K_s	L	ΔH	ΔK_s	ΔL	H	K_s	L
[1]	[2]	[3]	[4]	[5]	[6]	[7]	[8]	[9]	[10]	[11]	[12]	[13]	[14]	[15]	[16]
AB Aur[1]	IMS	163 ± 9	T[25], MSp[26]	70	32.6	489.0	5.062	4.23	3.254	...	2.09	...	...	⩽127	...
DM Tau[1,2]	LMS	145 ± 7	T[25]	19	5.8	435.0	9.757	9.522	9.458	10.0	...	...	⩽6.02	...	...
GM Aur[1]	LMS	160 ± 13	T[25]	28	16.0	480.0	8.603	8.283	8.369	0.759	...	...	⩽1.60	...	...
LkHα 330[2]	IMS	311 ± 24	T[25], 2Sp[27]	68		62.2	7.917	7.03	6.072	...	5.75	...	...	⩽96.8	...
HD100546[3–7]	IMS	110 ± 6	T[28], MSp[29]	13	11.0	88.0	5.962	5.418	4.201	0.251	...	...	⩽2.86	...	...
MWC 758[3,8,9]	IMS	160 ± 11	T[25], 2Sp[30]	73	16.0	176.0	6.56	5.804	4.599	...	0.100	1.58	...	⩽1.38	⩽17.9
SAO 206462[3,10]	IMS	136 ± 10	T[25], 2Sp[31]	46	13.6	272.0	6.587	5.84 3	5.04 6	0.02	0.100	...	⩽0.195	⩽0.957	...
HD169142[3,11,12]	IMS	114 ± 7	T[25], MSp[32]	20	11.4	114.0	6.911	6.41	5.995	0.132	0.132	...	⩽0.673	⩽0.528	...
TW Hya[2,3]	LMS	60.1 ± 2.5	T[25]	4	1.2	12.0	7.558	7.297	7.101	...	6.31	...	...	⩽3.10	...
HD 141569[13]	IMS	111 ± 1	T[33]	20	11.1	276.6	...	...	...	...	...	...	...	⩽30M_J at L-band	...
HD 142527[14]	IMS	157 ± 1	T[25]	140	31.4	471.0	5.715	4.980	4.280	...	...	...	439	235	81.2
PDS 70b[15,16]	LMS	113 ± 5	T[25]	60	17.0	113.0	8.823	8.542	8.026	...	0.631	1.74	...	0.351	0.418
PDS 70c[16]				...	...	...	8.823	8.542	8.026	...	0.302	2.29	...	0.168	0.546
LkCa 15b[1,17,18].	LMS	159 ± 8	T[25]	50	8.0	31.8	8.600	8.163	7.49	5.25	3.98	10.0	11.0	6.16	7.72
LkCa 15c[18]				...	...	...	8.600	8.163	7.49	5.25	3.98	10.0	9.70	6.16	...
FL Cha (T35)[19]	LMS	188 ± 10	T[34]	15	5.6	56.4	9.904	9.109	8.294	...	12.0	...	...	⩽10.9	...
FP Tau[2]	LMS	128 ± 7	T[35]	...	6.4	25.6	9.175	8.873	8.38	...	17.4	25.1	...	⩽9.14	⩽5.59
DZ Cha[20]	LMS	100.83 ± 0.26	T, 2Sp[27]	7	4.0	80.7	...	...	...	ΔJ=8.5	...	...	...	...	...
RX J1604.3-2130A[1,21]	LMS	150 ± 8	T[25]	70	15.0	450.0	9.103	8.506	7.548	0.016	0.0158	...	⩽.0186	⩽.016	...
RXJ1615.3-3255[2]	LMS	158 ± 6	T[25]	30	3.2	31.6	8.777	8.558	8.528	...	11.0	...	...	⩽11.6	...
RXJ1842.9-3532[2]	LMS	154 ± 7	T[34]	160	6.2	30.8	8.709	8.17	7.673	...	6.31	...	...	⩽9.10	...
DoAr44[2]	LMS	146 ± 8	T[25]	30	2.9	29.2	8.246	7.61	6.794	...	10.0	...	...	⩽21.7	...
IM Lup[1]	LMS	158 ± 8	MSp[36]	...	31.6	474.0	8.089	7.739	6.938	1.20	...	...	⩽4.01	...	...
V1247 Ori[1,2,22]	IMS	398 ± 25	1Sp[37]	...	39.8	1194.0	8.203	7.408	6.344	0.912	8.32	3.63	⩽17.3	⩽162	⩽50.7
DN Tau[1]	LMS	128 ± 7	...	...	12.8	384.0	8.342	8.015	7.716	1.91	...	...	⩽3.30	...	...
GO Tau[1]	LMS	145 ± 7	...	...	14.5	435.0	9.776	9.332	9.006	19.1	...	...	⩽11.2	...	...
DL Tau[1]	LMS	159 ± 8	...	...	31.8	477.0	8.679	7.96	6.973	...	1.74	...	...	⩽3.26	...
MWC 480[1]	IMS	162 ± 12	...	...	32.4	486.0	6.262	5.527	4.913	0.631	...	...	⩽11.8	...	...
CI Tau[1]	LMS	159 ± 8	FD, rings[38]	...	31.8	477.0	8.431	7.793	6.775	2.75	...	...	⩽6.72	...	...
HD163296[23]	IMS	101 ± 12	FD, rings[39]	...	20.2	303.0	5.531	4.779	3.706	...	...	1.00	...	...	⩽10.3
HL Tau[24]	LMS	140 ±	FD, rings[40]	...	28.0	168.0	9.171	7.41	5.298	...	...	1.00	...	...	⩽4.52
DoAr 21[2]	LMS	134 ± 9	DD[41]	100	2.7	26.8	6.862	6.227	5.783	...	19.1	...	...	⩽125	...
TYC 4496-780-1[1]	IMS	180 ± 12	...	...	36.0	540.0	7.758	7.57	7.159	3.31	...	...	⩽19.3	...	...
IRAS 04028+2948[1]	IMS	344 ± 13	...	...	34.4	1032.0	9.472	8.831	7.722	27.5	...	...	⩽121	...	...
V1075 Tau[1]	LMS	143 ± 7	...	...	14.3	429.0	9.056	8.85	8.733	0.302	...	...	⩽0.339	...	...
V1076 Tau[1]	LMS	151 ± 7	...	...	15.1	453.0	9.460	9.308	9.148	0.575	...	...	⩽0.492	...	...
V397 Aur[1]	LMS	149 ± 18	...	...	14.9	447.0	8.317	8.129	8.074	3.98	...	...	⩽9.46	...	...
V1207 Tau[1]	LMS	125 ± 6	...	...	12.5	375.0	8.960	8.802	8.734	2.09	...	...	⩽1.94	...	...

Table 1
(Continued)

Star	Type	Distance	Morphology[a]	Cavity Size	Inner Extent	Outer Extent	Stellar Magnitude			Contrast			λL_λ		
										$(10^{-3}$ Magnitudes$)$			$(10^{30}$ erg s$^{-1})$		
		(pc)		(au)	(au)	(au)	H	K_s	L	Δ H	ΔK_s	ΔL	H	K_s	L
[1]	[2]	[3]	[4]	[5]	[6]	[7]	[8]	[9]	[10]	[11]	[12]	[13]	[14]	[15]	[16]
HIP 77545[1]	IMS	151 ± 8	⋯	⋯	30.2	453.0	7.996	7.895	7.829	0.331	⋯	⋯	⩽1.09	⋯	⋯
HIP 79462[1]	IMS	152 ± 7	⋯	⋯	30.4	456.0	7.429	7.294	7.261	0.912	⋯	⋯	⩽5.15	⋯	⋯
HIP 80088[1]	IMS	144 ± 8	⋯	⋯	28.8	432.0	7.904	7.785	7.728	0.832	⋯	⋯	⩽2.71	⋯	⋯
LkCa 19[1]	LMS	160 ± 13	DD[34]	190	16.0	480.0	8.318	8.148	8.058	2.75	⋯	⋯	⩽7.55	⋯	⋯

Note. [1] Uyama et al. (2017), [2] Willson et al. (2016), [3] Cugno et al. (2019), [4] Quanz et al. (2013), [5] Sissa et al. (2018), [6] Currie et al. (2017), [7] Follette et al. (2017), [8] Grady et al. (2013), [9] Reggiani et al. (2018), [10] Maire et al. (2017), [11] Gratton et al. (2019), [12] Ligi et al. (2018), [13] Mawet et al. (2017), [14] Christiaens et al. (2018), [15] Keppler et al. (2018), [16] Haffert et al. (2019), [17] Kraus & Ireland (2012), [18] Sallum et al. (2015), [19] Cieza et al. (2013), [20] Canovas et al. (2018), [21] Canovas et al. (2017), [22] Kraus et al. (2013), [23] Guidi et al. (2018), [24] Testi et al. (2015), [25] Espaillat et al. (2014b), [26] Tang et al. (2017), [27] Akiyama et al. (2016), [28] Grady et al. (2001), [29] Follette et al. (2017), [30] Grady et al. (2013), [31] Muto et al. (2012), [32] Gratton et al. (2019), [33] Malfait et al. (1998), [34] van der Marel et al. (2016), [35] Currie & Sicilia-Aguilar (2011), [36] Avenhaus et al. (2018), [37] Dong et al. (2018a), [38] Clarke et al. (2018), [39] Zhang et al. (2016), [40] ALMA Partnership et al. (2015), [41] Jensen et al. (2009)
[a] Transition disks are indicated by T, debris disks by DD, and full disks by FD. One-armed, two-armed, and multiarmed spirals are indicated by 1Sp, 2Sp, and MSp respectively. Disks with imaged ring structure are indicated by rings.

20.6 ± 1.2 and 34.5 ± 2.0 au (Haffert et al. 2019). The companions have been imaged in the NIR (Keppler et al. 2018) and Hα (Wagner et al. 2018; Haffert et al. 2019), and their associated circumplanetary disks may have been discovered in millimeter continuum emission (Isella et al. 2019). From their Hα measurement, Wagner et al. (2018) estimated a planetary accretion rate of $10^{-11\pm1} M_\odot \text{ yr}^{-1}$. A weak-lined T Tauri star, PDS 70 has an Hα equivalent width of ~ 2 Å (Gregorio-Hetem & Hetem 2002). Adopting the stellar parameters presented in Long et al. (2018) and the prescription for converting line luminosity to accretion luminosity given in Fang et al. (2009), we arrive at a stellar accretion rate of $8 \times 10^{-11} M_\odot \text{ yr}^{-1}$. For such low rates of accretion, it is possible that most of the Hα emission arises from chromospheric activity, so this accretion rate should be taken as an upper limit. Over 5 Myr, only $0.4 M_J$ would be accreted by the star at this rate. If they are hot start planets, the masses of PDS 70b and PDS 70c are estimated to be 4–17 and 4–12 M_J, respectively (Haffert et al. 2019), and the accretion rate would have been substantially higher in the past. There are significant uncertainties in both the planetary and stellar accretion rates, yet the derived values are consistent with a reasonable fraction of the accreting material through the disk being captured by the planet.

Multiple orbiting planetary companions have been reported in association with LkCa 15 (Kraus & Ireland 2012; Sallum et al. 2015), its three planetary candidates detected at ~ 15–20 au in the inner cavity of its disk using NIR sparse aperture masking (SAM; Sallum et al. 2015). One of these sources has been imaged in Hα, from which the accretion rate onto the planet has been estimated. The IR colors and Hα emission are consistent with a planet mass times accretion rate $M_p \dot{M}_p \sim (3 - 10) \times 10^{-6} M_J^2 \text{ yr}^{-1}$. For a Jupiter mass companion, this translates to an accretion rate of $\sim (3 - 10) \times 10^{-9} M_\odot \text{ yr}^{-1}$, which is within a factor of a few of the stellar accretion rate measured for LkCa 15 ($3.6 \times 10^{-9} M_\odot \text{ yr}^{-1}$; Ingleby et al. 2013). A subsequent study found that the Hα luminosity of the companion appears to vary, indicating variable accretion (Mendigutía et al. 2018). While there is significant uncertainty about the accretion rate onto the planet, the derived values are largely consistent with the expectation that a nonnegligible fraction of the mass accreting through the disk makes it across the planet's orbit into the inner disk (Lubow & D'Angelo 2006). While the detection of orbital motion in data taken over 6 yr supports the interpretation that the emission arises from massive planetary companions (Sallum et al. 2015; S. Sallum et al. 2020, in preparation), other studies of LkCa 15 that use direct imaging techniques rather than SAM find structures that are more consistent with emission from an inner disk (Thalmann et al. 2016; Currie et al. 2019). Further study is needed to understand the properties of the orbiting emission sources.

One or more circumplanetary disks may have been detected in the HD 100546 system (Liskowsky et al. 2012; Brittain et al. 2013, 2014, 2015; Quanz et al. 2013; Currie et al. 2015, 2017; Brittain et al. 2019). This system hosts a source of 5 μm CO fundamental emission located ~ 12 au from the star, close to the inner rim of the outer disk, whose orbit has been followed for 15 yr. The CO flux is consistent with emission from a circumplanetary disk with a radius of ~ 0.3 au if we assume the emitting gas is optically thick and at the same temperature as the circumstellar gas near the disk edge

(1400 K; Brittain et al. 2013). The temperature and emitting area are consistent with the theoretically predicted thermal properties of circumplanetary disks surrounding giant planets. Szulágyi et al. (2014) reported a disk temperature of ~ 2000 K out to a Hill radius $R_{\text{Hill}} \sim 0.8$ au for their case of a 10 M_J planet at 5 au (see also Szulágyi 2017; Szulágyi & Mordasini 2017). Similar temperatures have been reported for the inner circumplanetary disk in other three-dimensional radiation hydrodynamical simulations (Klahr & Kley 2006; Gressel et al. 2013).

Confirmation of this source by direct imaging remains ambiguous. Currie et al. (2015) reported the possible presence of a point source at the expected location of the CO emission, although the point source was not confirmed in subsequent observations (Follette et al. 2017; Rameau et al. 2017). One reason for the differing results may be because the point source fell behind the coronagraphic mask in the later observations (Currie et al. 2017). Attempts to detect the source with Atacama Large Millimeter/submillimeter Array (ALMA) continuum imaging have also failed (Pineda et al. 2019), although it is likely that the pressure bump at the inner edge of the outer disk strongly filters out millimeter-sized dust grains and prevents them from reaching the circumplanetary disk. Moreover, grains that make it to the circumplanetary disk are expected to drift inward quickly (Zhu et al. 2018), enhancing the gas-to-dust ratio of the circumplanetary disk and leading to weak millimeter continuum emission. Thus, the status of this third possible planet remains uncertain. In addition to the source at ~ 12 au, an extended source of IR emission has been reported at ~ 50 au (Quanz et al. 2015), and an additional millimeter continuum point source has been detected at 5.6 au with ALMA (Pérez et al. 2019).[6]

In summary, among the 20 sources studied to date that show signposts of giant planets (large cavities or two-arm spirals), accreting gas giant planets have been detected in at least one young LMS system (PDS 70) and possibly one additional young LMS system (LkCa 15) and one young IMS system (HD 100546; Table 2). These results correspond to a detection rate of 5%–15% among this select group, whereas we would have expected to detect one or more giant planet companions in every system if all transition disks host multiple high-mass giant planets that radiate away their accretion energy as they form. In addition, no planetary companions have been reported in association with the remaining 20 nontransition disk sources in Table 1.

These results indicate that the incidence rate of bright, detectable giant planet companions among all stars is very low. That is, among young LMSs, only 5%–15% of their protoplanetary disks have transition disk SEDs (e.g., Muzerolle et al. 2010; Furlan et al. 2011), and of the 12 young LMS transition disks in Table 1, only one, possibly two, have a bright detected companion, for a detection rate of 8%–16%. The product of these two rates implies an incidence rate of accreting giant planetary companions to young LMSs of $\sim 1\%$. Similarly, among IMS protoplanetary disks, $\sim 40\%$ have transition disk SEDs (see S. D. Brittain & J. R. Najita et al. 2020, in preparation) and $\sim 20\%$ have two-arm spirals (Dong et al. 2018b), whereas none or possibly one (HD 100546) of the eight young IMS transition disks in Table 1 have a bright

---

[6] A companion candidate has very recently been detected in LBT L'- and M-band imaging of the MWC 758 disk (Wagner et al. 2019). Assuming the emission is entirely photospheric, the planet is estimated to be 2–5 M_J in mass in a hot start scenario. No accretion signature has been detected from the candidate so far. As confirmation of the candidate is currently underway (K. Wagner 2020, private communication), we do not include this candidate in our study.

detected companion, for a detection rate of 0%–12%. The product of these two rates implies an incidence rate of accreting giant planets of 0%–5% for young IMSs. In other words, the incidence rate of accreting giant planet companions among all protoplanetary disks is likely of the order of a few percent.

3. Toy Model of Episodic Accretion

It is perhaps surprising that the planet detection rate at these very young ages is so low, especially if most forming planets radiate away their accretion energy as they form (i.e., they are cold start planets) and are expected to be bright in their mass-building phase. Here we explore the role episodic accretion may play in accounting for the dearth of bright young systems observed among these disks.

Lubow & Martin (2012) have noted that circumplanetary disks, like the more extended circumstellar disks in which they reside, are likely to harbor significant dead zones, i.e., regions that are insufficiently ionized to participate in accretion via the magnetorotational instability (MRI). As a result, as it is fed material from the circumstellar disk, the circumplanetary disk will grow in mass until it becomes gravitationally unstable. By driving turbulent heating (and thus ionization), gravitational instability warms the disk until it is sufficiently ionized thermally to drive accretion via the MRI, a process they refer to as the gravomagneto instability (Armitage et al. 2001; Zhu et al. 2009; Martin & Lubow 2011). Their model predicts outburst rates ranging from 0.04 to 2 M_J yr^{-1} and quiescent rates ranging from 4×10^{-7} to $3 \times 10^{-5} M_J$ yr^{-1}, with accretion outbursts that last for several years occurring every 10^4–10^5 yr (Lubow & D'Angelo 2006).

To compare the observed properties of detected accreting giant planets with the predictions of episodically accreting circumplanetary disks, we extend the work of Lubow & Martin (2012) by considering the effect of non-steady-state disk accretion and the growing mass of the planet. To set the rate at which the circumplanetary disk is fed, we first consider a circumstellar disk with an accretion rate that declines with time as $t^{-3/2}$, mimicking the decline in the average measured stellar accretion rate over megayear timescales[7] (see, for example, Sicilia-Aguilar et al. 2005), such that

$$\dot{M}(t) = \dot{M}(t_0)(t/t_0)^{-3/2}. \tag{1}$$

We adopt $t_0 = 1$ Myr and an initial accretion rate of $\dot{M}(t_0) = 10^{-8}$ $M_\odot$ yr^{-1}, an accretion rate typical of young T Tauri stars (e.g., Hartmann et al. 1998). We then embed in the circumstellar accretion disk a forming giant planet with a mass $M_p = 20 M_\oplus$, roughly the mass at which runaway accretion begins (e.g., D'Angelo et al. 2010).

From a theoretical perspective, the fraction of the accreting circumstellar disk material that is captured by the planet, $f(M_p)$, depends on a variety of parameters, including q, the mass ratio of the planet and star, the orbital eccentricity of the companion, and the viscosity of the gas. Estimates from two-dimensional simulations indicate that a forming gas giant planet captures 75%–90% of the accreting material (Lubow & D'Angelo 2006).

However, the value is uncertain because the flow onto the planet and circumplanetary disk is intrinsically three-dimensional (Ayliffe & Bate 2012; Tanigawa et al. 2012; Fung et al. 2015; Szulágyi et al. 2016; Batygin 2018).

Observationally, there are few constraints on the captured fraction, although we might attempt to infer its typical value from the ratio of the stellar and planetary accretion rates for the few accreting companions detected to date. As described in Section 2, the properties of the accreting companions to LkCa 15 and PDS 70 indicate that a significant portion of the material accreting through the disk is captured by the companion (~50% and ~10%, respectively), while only a small fraction of the mass is captured in the case of the companion to HD 142527 (~10^{-3}). These values are uncertain because the scaling relationship between Hα emission and planetary accretion rate may be in error, the accretion onto the planet may not be in steady state (e.g., Mendigutía et al. 2018), and/or the Hα line may be more heavily extincted by circumplanetary matter than estimated.

Given the uncertainties surrounding the captured fraction, we parameterize it as

$$f(M_p) = \frac{1}{1 + a/q}, \tag{2}$$

where a is a free parameter, and $q = M_p/M_\star$ is the ratio of the companion mass to the mass of the central star. We arrived at this functional form and the value $a = 10^{-4.5}$ by fitting the relationship between f and q found in the two-dimensional hydrodynamical simulations presented by Lubow & D'Angelo (2006). Here we explore how the efficiency factor affects the duty cycle of accretion outbursts.

As material is captured by the forming planet, it fills a circumplanetary disk, which accretes onto the planet at a rate that depends on ζ, the mass ratio of the circumplanetary disk to the forming planet. Here we assume

$$\dot{M}_P = 5 \times 10^{-4} M_J \text{ yr}^{-1}; \text{ for } \zeta \gtrsim 0.1$$
$$= 5 \times 10^{-8} M_J \text{ yr}^{-1}; \text{ for } \zeta \lesssim 0.1. \tag{3}$$

Although these rates are highly uncertain as well, they are based on measured accretion rates for young stars. While Lubow & Martin (2012) adopted much higher accretion rates in their outburst, Hall et al. (2019) found that in their models for marginally gravitationally unstable disks, the accretion rate is of order 10^{-7} $M_\odot$ yr^{-1}, which we adopt for our model.

In quiescence, we assume that the accretion rate onto the planet is reduced by 4 orders of magnitude, consistent with the models of Lubow & Martin (2012). We allow the model to run until $q = 5 \times 10^{-3}$, at which point the forming companion halts accretion onto its circumplanetary disk (Lubow et al. 1999; Lubow & D'Angelo 2006).

With these assumptions, the planet grows to 9 M_J in about 3 Myr (Figure 1). The accretion luminosity of the planet alternates between ~4×10^{-5} and ~$0.4 L_\odot$. Outbursts occur every 1500 yr and last ~30 yr; thus, the circumplanetary disk spends ~2% of the runaway accretion phase undergoing an outburst (Figure 1). Even in quiescence, the accretion luminosity exceeds the luminosity of a cold start planet (~$10^{-6} L_\odot$; Fortney et al. 2008). We can compare the accretion luminosity to the integrated luminosity of the detected companions orbiting HD 142527, LkCa 15, and PDS 70. We fit the disk accretion models by Zhu (2015) to the measured

---

[7] As noted by Hartmann et al. (2016), although measured stellar accretion rates follow this declining trend, at stellar ages beyond ~3 Myr, most young stars have undetectable accretion. Our assumed rate of decline therefore overestimates the stellar accretion rate at late times, although this flaw has little impact on our results qualitatively. The effect of a steeper decline in the accretion rate is to fill the circumplanetary disk more slowly at later times, resulting in more time between outbursts.
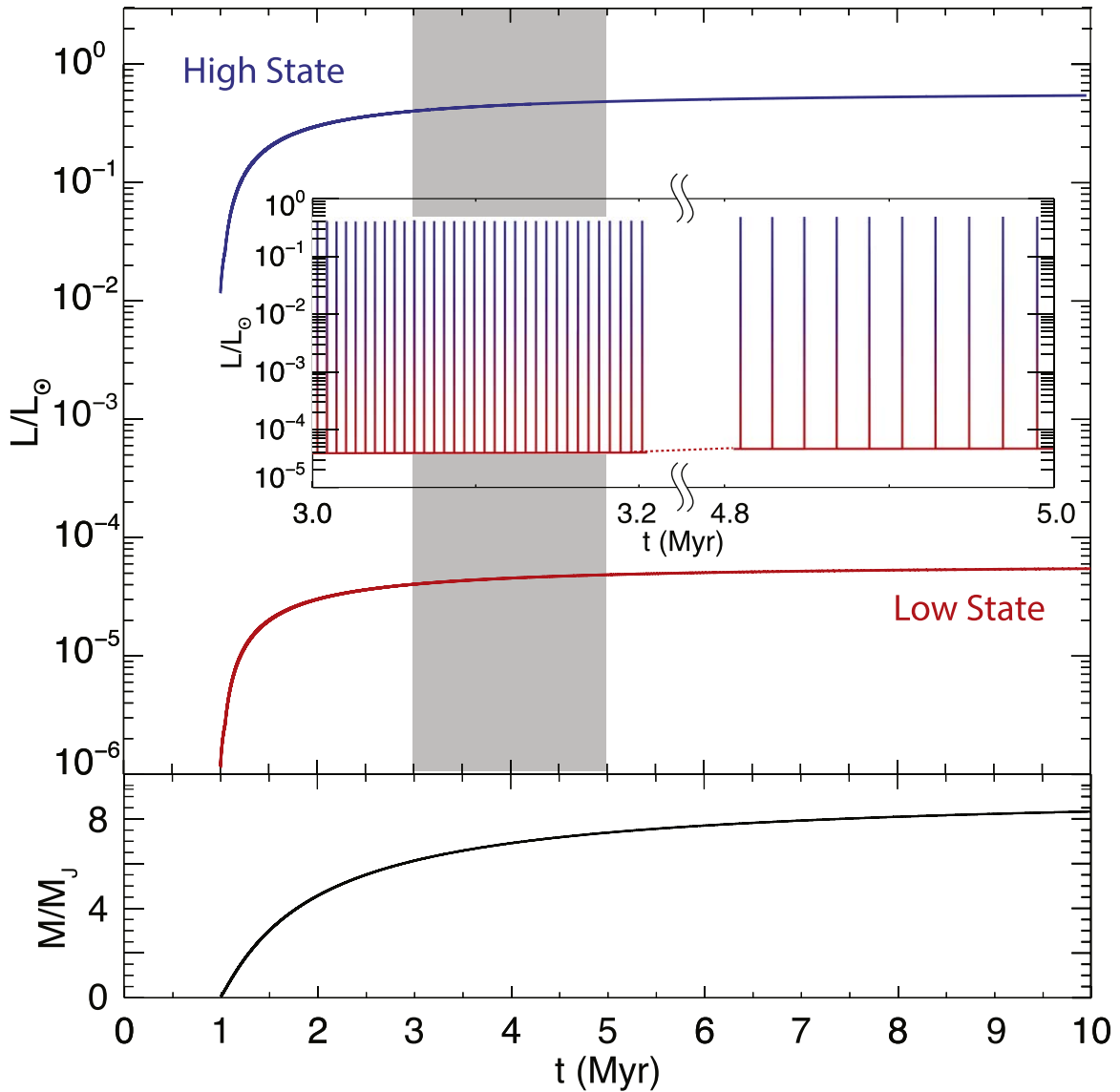
Figure 1. Accretion luminosity (upper panel) and planetary mass (lower panel) as a function of time. The accretion luminosity increases with planetary mass and alternates between quiescence (red curve) and outburst (blue curve). The inset shows an enlarged version of the shaded region of the plot. When the planet mass is low and the circumstellar disk accretion rate is high, outbursts are more frequent as the circumplanetary disk grows in mass to $0.1\,M_p$ more frequently. However, the potential well is not as deep and the accreted mass is lower, so the luminosity of the accretion is lower. As the planet grows in mass and the circumstellar disk accretion rate declines, the outbursts become less frequent but more intense. In the model shown, the planet mass grows to $\sim 8\,M_J$ in 5 Myr and continues to grow until the circumstellar disk ceases to feed the circumplanetary disk and the circumplanetary disk empties all of its mass onto the central object.

Table 2
Stars with Accreting Companions Imaged

Star	Mass	dist (pc)	Stellar Magnitude			Contrast (10^{-3} Magnitudes)			λL_λ (10^{30} erg s^{-1})		
			H	K_s	L	ΔH	ΔK_s	ΔL	H	K_s	L
HD 142527[1]	IMS	157 ± 1	5.715	4.980	4.280	⋯	⋯	⋯	439	235	81.2
LkCa 15b[2,3,4]	LMS	159 ± 8	8.600	8.163	7.49	5.25	3.98	10.0	11.0	6.16	7.72
LkCa 15c[4]	LMS	159 ± 8	8.600	8.163	7.49	5.25	3.98	10.0	9.70	6.16	⋯
PDS 70b[5,6]	LMS	113 ± 5	8.823	8.542	8.026	⋯	0.631	1.74	⋯	0.351	0.418
PDS 70c[6]	LMS	113 ± 5	8.823	8.542	8.026	⋯	0.302	2.29	⋯	0.168	0.546

Note. [1] Christiaens et al. (2018), [2] Uyama et al. (2017), [3] Kraus & Ireland (2012), [4] Sallum et al. (2015), [5] Keppler et al. (2018), [6] Haffert et al. (2019)

photometry for each source (Figure 2) and find that their luminosities range from 10^{-4} to $0.6\,L_\odot$ (see Table 3 for the properties of the companions). The gray bars in Figure 2 show

the range of upper limits on λL_λ of the sample in Table 1. Adopting the colors from the Zhu (2015) model, we find that the published observations are sufficiently sensitive to detect
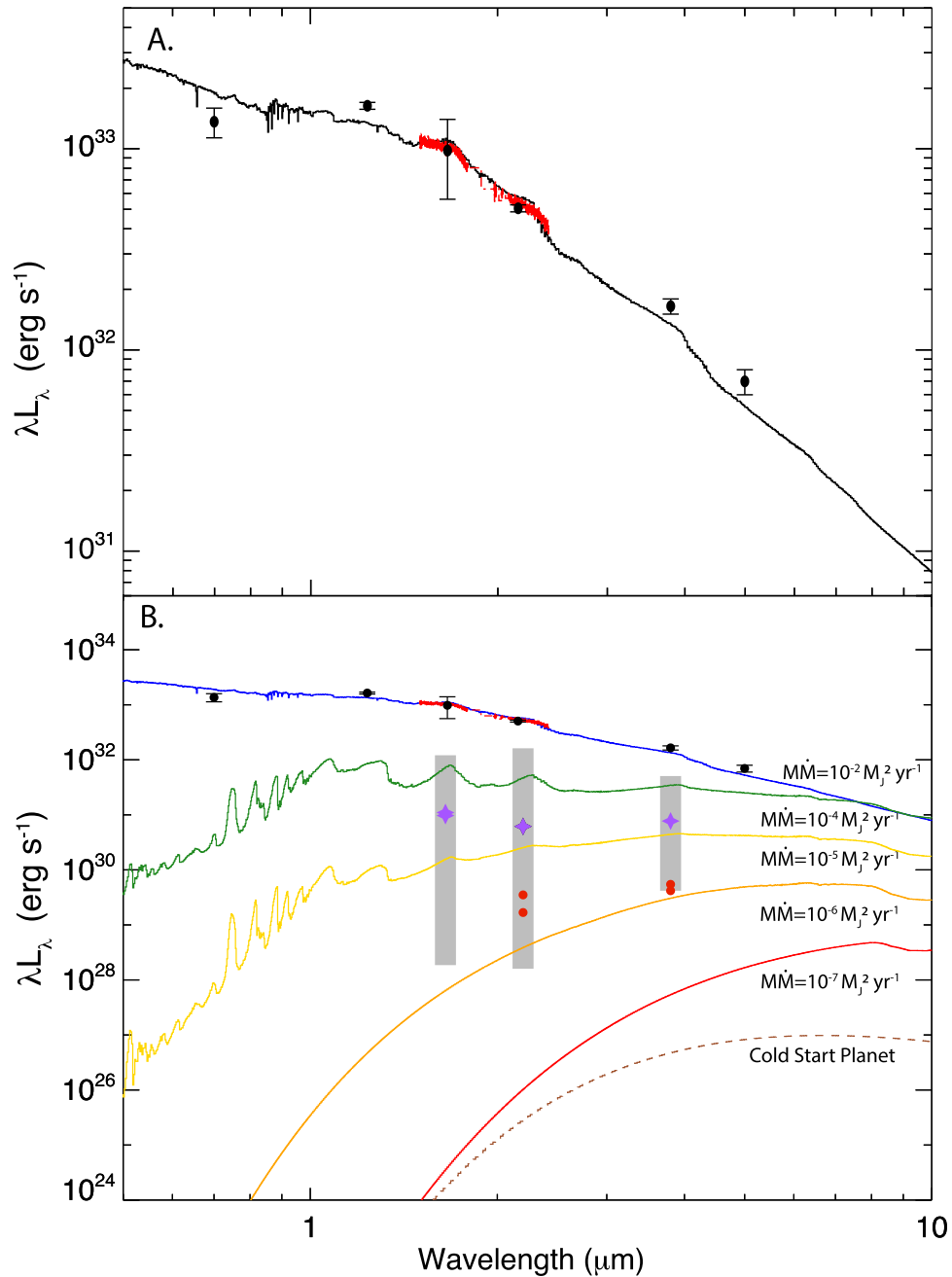
Figure 2. Photometry of HD 142527B and models of active circumplanetary disks. The photometry of the companion orbiting HD 142527 is corrected for the circumplanetary disk inclination and reddening following Zhu (2015) assuming an inclination of 70°, $A_J = 1.6$, and $\alpha = 1.7$. With these parameters, the photometry of the companion is well fit by a model of an active disk with $M\dot{M} = 10^{-2}\, M_J^2\, yr^{-1}$, $R_{in} = 1.5\, R_J$, and $R_{out} = 15\, R_J$ (panel a). In panel b, we replot the photometry from HD 142427b, as well as the photometry of the candidate planets orbiting LkCa 15 (purple stars) and PDS 70 (red circles). The range of observational limits from the literature are shown as vertical gray bars. We also plot the SED of an accreting circumplanetary disk for four additional accretion rates, as well as the spectrum of a 550 K blackbody representing a cold start 1 Myr old 1 M_J planet. Previous observations are not sensitive enough to have detected a gas giant planet with a quiescent disk ($M\dot{M} < 10^{-6}\, M_J^2\, yr^{-1}$).

accreting circumplanetary disks with an integrated luminosity of 10^{-4}–0.1 $L_\odot$.

Thus, studies to date have imaged 20 disks with transition disk SEDs (four of which have two-arm spirals) with sufficient sensitivity to detect a companion as bright as $0.1\, L_\odot$ (see Section 2). If each of the 20 disks harbors one accreting gas giant planet, and their circumplanetary disks are in outburst 2% of the time, we have a 33% chance of catching one or more circumplanetary disks in outburst. Dodson-Robinson & Salyk (2011) argued that the large cavity sizes of transition disks

required the presence of multiple multi-Jupiter mass planets within the optically thin region. If each transition disk harbors two (three) accreting planets (and the observations probe the orbital radii of both/all planets), we have a 55% (70%) chance of catching one or more planets in outburst.

Interestingly, one companion as bright as our outburst luminosity (~0.6 $L_\odot$) has been detected to date: HD 142527B. In Section 4 we explore the possibility that HD 142527B is a planet surrounded by a circumplanetary disk in outburst. More generally though, the toy model suggests that episodic

Table 3
Companion Data

Star	a (au)	M (M_J)	MM˙ (M_J^2 yr^{-1})	$L/L_\odot$
HD 142527B[1]	22^{+19}_{-11}	270^{+170}_{-150}	10^{-2} [4]	0.6
LkCa 15b[2]	14.7 ± 2.1	$\leqslant 10$	10^{-5}	$\sim 10^{-3}$
LkCa 15c[2]	18.6 ± 2.5	$\leqslant 10$	10^{-5}	$\sim 10^{-3}$
PDS 70b[3]	20.6 ± 1.2	4–17	0.3–9×10^{-7}	$\sim 10^{-4}$
PDS 70c[3]	34.5 ± 2.0	4–12	0.15–6×10^{-7}	$\sim 10^{-4}$

Note. [1] Christiaens et al. (2018), [2] Sallum et al. (2015), [3] Haffert et al. (2019), [4] MM˙ is estimated by assuming that luminosity of the companion object is dominated by the accretion luminosity and that the radius of the companion is $1.5R_J$.

accretion can plausibly explain the low detection rate of accreting planetary companions to young stars. Future observational constraints on the incidence rate of giant planets and their luminosity in the accretion phase can directly constrain the duty cycle of episodic accretion and the outburst accretion rate.

In the episodic accretion picture, forming planets present two faces to the world. Most of the time, they are accreting very slowly, and they look like a faint cold start planet surrounded by a quiescent disk. A small fraction of the time (a few %), when in outburst, the emission from the system is dominated by emission from the disk, as in an FU Ori object, with the color and luminosity of an M star. In the next section, we discuss whether the directly imaged companion to HD 142527 could be in the latter state.

4. HD 142527: Stellar or Planetary Companion?

The directly imaged companion to the young F6 star HD 142527 ($2.0 \pm 0.3\,M_\odot$) has been detected through its NIR continuum and Hα emission at a separation of $\sim$13 au from the star (Biller et al. 2012; Close et al. 2014). A spectrum of the companion in the H and K bands has also been acquired (Christiaens et al. 2018). These observations have been interpreted as emission from a young M2.5 star with a mass of $\sim$0.1–0.4 $M_\odot$ that is accreting at a rate $6 \times 10^{-10}\,M_\odot$ yr^{-1} (Biller et al. 2012; Close et al. 2014; Lacour et al. 2016; Christiaens et al. 2018), a tiny fraction of the accretion rate onto this 5.0 ± 1.5 Myr old star ($\sim 2 \times 10^{-7}\,M_\odot$ yr^{-1}; Mendigutía et al. 2014).

Studies that have used dynamical arguments to constrain the mass of the companion favor a stellar companion, although the constraints admit the possibility of one or more planetary mass companions instead (Price et al. 2018; Claudi et al. 2019; see Section 5 for further details). In the absence of strong evidence to the contrary, we here consider the possibility that the companion is a planetary mass companion surrounded by a circumplanetary disk undergoing an accretion outburst. Earlier studies have suggested that the NIR spectrum of an active accretion disk can mimic that of an M star (e.g., Herbig 1977; see also Zhu 2015).

Figure 2(a) compares the IR photometry of the companion (black points; Lacour et al. 2016) with the model spectrum of an accreting circumplanetary disk (black line). In the model, the circumplanetary disk accretes at a constant rate onto the planet. The effective temperature of the circumplanetary disk is

the standard steady optically thick accretion disk temperature. The vertical temperature dependence of the disk atmosphere at each radius is calculated using the gray-atmosphere approximation in the Eddington limit, adopting the Rosseland mean optical depth. With the temperature determined at each radius, the SED of the local annulus is calculated. By summing the SEDs from different annuli, the SED of the accretion disk is obtained (Zhu 2015).

The other model parameters—in addition to the disk accretion rate and the range of disk radii that contribute to the emission—are the disk inclination and the reddening to the disk. The inclination of the outer disk around HD 142527 is $\sim$20°–30° (Pontoppidan et al. 2011; Casassus et al. 2013), whereas the inner circumstellar disk is inferred to have an inclination of $\sim$70° relative to the outer disk (Marino et al. 2015). If the companion has a disk, it is not clear what the orientation of the disk would be, so its inclination is treated as a free parameter in our fit. The planet and circumplanetary disk are expected to be embedded in a circumplanetary envelope (Tanigawa et al. 2012; Gressel et al. 2013; Szulágyi et al. 2016) that may extinct and redden the emission from the planet+disk by an unknown amount. We therefore assume a parameterized reddening law $A_\lambda = A_J (\lambda/1.235)^{-\alpha}$, where A_J and α are free parameters.

In the model calculation, the inclination correction is treated simply as a multiplicative factor that corrects for the projected disk emitting area. We obtain a reasonable fit with a disk that extends from an inner radius of $R_{in} = 1.5R_J$ to an outer radius of $R_{out} = 15R_J$; an accretion rate $\dot{M}_p$, such that $M_p\dot{M}_p = 10^{-2}\,M_J^2$ yr^{-1}, where M_p is the planetary mass; and extinction and inclination parameters of $A_J = 1.6$, $\alpha = 1.7$, and $i = 70°$ (Figure 2). In this model the temperatures of the disk extend from $\sim$10,000 K at R_{in} to $\sim$1,600 K at R_{out}.

To compare the model to the NIR spectrum of the companion (Christiaens et al. 2018), we assume that the absolute flux calibration of the photometry is more reliable than the spectrum, so we scale the spectrum to be consistent with the photometry. The model and scaled spectrum agree well (Figure 2), although there is a slight discrepancy in the K-band region. Such differences are not surprising because of the simple assumptions made in the model. For example, the model assumes a simple vertical temperature structure (based on a gray atmosphere with no temperature correction; Zhu 2015). Any deviation from the standard radial disk temperature profile assumed here will also alter the SED. Furthermore, the opacity of the model is fixed at solar abundance and an adopted mean opacity, so any changes in the elemental composition of the accreting material would affect the SED. For example, any trapping of large grains in pressure bumps in the circumstellar disk will reduce the dust content of the material accreting into the circumplanetary disk.

These results show that the emission properties of the companion to HD 142527 are plausibly those of a giant planet surrounded by a circumplanetary disk that is undergoing an accretion outburst and whose emission dominates the emission from the planet. If the companion is in fact a 10 M_J planet surrounded by a circumplanetary disk, then our fit value of $M_p\dot{M}_p = 10^{-2}\,M_J^2$ yr^{-1} implies a planetary accretion rate of $10^{-6}\,M_\odot$ yr^{-1}, roughly an order of magnitude higher than the stellar accretion rate for this system (Mendigutía et al. 2014).

5. Discussion

In Section 1, we argued that the high incidence rate of disk substructure indicating the presence of massive ($\sim 5\,M_J$) giant planets (e.g., two-arm spirals and transition disk morphologies associated with $\sim 10\%$–20% of disk-bearing stars), coupled with the lack of directly imaged hot start planets in this mass range at >10 Myr ages, suggests that giant planets form by cold start, i.e., that planets radiate away much their accretion energy in the accretion phase. The lack of evidence for energy loss in this form, i.e., the ready detection of bright, accreting planets in the pre-main-sequence phase (~ 1 Myr), led us to propose that planets accrete their mass episodically, through punctuated outbursts of accretion in the runaway gas accretion phase.

This interpretation may appear too glib when we consider that some of the first directly imaged planets, those orbiting β Pic and HR 8799, appear to be hot start planets. Dynamical constraints on their masses, coupled with their observed luminosities, are consistent with the predictions of hot start models (Fabrycky & Murray-Clay 2010; Wang et al. 2018). While these planets were first reported many years ago (Marois et al. 2008; Lagrange et al. 2009), subsequent discoveries of directly imaged planets have been few and far between (Bowler 2016; Stone et al. 2018; Nielsen et al. 2019).

One interpretation of the discrepancy between these results is that planet formation proceeds through multiple pathways, resulting in a range of initial conditions spanning a cold start to a hot start (Spiegel & Burrows 2012). Planet formation via gravitational instability, which favors high-mass planets ($>10\,M_J$), is expected to produce hot start planets, while core accretion, which favors low-mass planets ($<10\,M_J$), is expected to produce colder-start planets. Both pathways may lead to 5–15 M_J planets at the orbital separations probed by direct imaging, with the brighter hot start planets readily detected (β Pic, HR 8799) and the (possibly more numerous) cold start planets as yet unprobed.

The episodic accretion scenario described in Section 3 predicts that accreting planets will come in two flavors: (1) outbursting systems with such high disk accretion rates that their emission is dominated by the circumplanetary disk and has the color of LMSs and (2) systems that are faint because the circumplanetary disk is inactive. At a planet mass of $\sim 3M_J$—the mass of the multiple planets invoked by Dodson-Robinson & Salyk (2011) to explain the large cavities of transition disks—the outbursting state in our toy model corresponds to $M_p\dot{M}_p = 1.5 \times 10^{-3}\,M_J^2\,\mathrm{yr}^{-1}$ and is sufficiently bright to have been detected by the 40 published observations of disks (Figure 2; Table 1). The quiescent state for such a $3M_J$ planet corresponds to $M_p\dot{M}_p = 1.5 \times 10^{-7}\,M_J^2\,\mathrm{yr}^{-1}$, or about 2 orders of magnitude fainter at the K band than the most sensitive published observations to date (Figure 2). As with young stars, there is likely a large range of accretion rates that represent the quiescent, steady-state rate of circumplanetary disks. Because quiescent disks are faint in the NIR and emit more of their energy in the mid-IR, searches at longer wavelengths may be better able to detect quiescent disks (Figure 2; see also Szulágyi et al. 2019).

While the emission properties of HD 142527b are plausibly consistent with those of a circumplanetary disk in outburst (Figure 2), the companions PDS 70bc and LkCa 15bc have fluxes between the outburst and quiescent states of our model. We hypothesize that these values reflect the upper limit of the range of quiescent states rather than the lower range for

outbursting disks, because it is unlikely that two circumplanetary disks in a given system would undergo an outburst simultaneously.

Other authors have described how the HD 142527 system properties are consistent with a stellar, rather than planetary, companion (e.g., Biller et al. 2012; Lacour et al. 2016; Christiaens et al. 2018). A stellar companion is consistent with many detailed aspects of the system: the multiple spiral arms in the outer disk at $r \gtrsim 100$ au (Fukagawa et al. 2006; Canovas et al. 2013), the large central clearing in the disk ($\sim 1''$ radius; Fukagawa et al. 2013), the azimuthal asymmetry in the outer disk (Casassus et al. 2013), and evidence for a (spatially unresolved) inner disk that is highly misaligned with the outer disk (Marino et al. 2015). Price et al. (2018) proposed that these properties can be explained by a single companion that has a mass of 0.4 $M_\odot$ and an unusual orbit with both high eccentricity ($e = 0.6$–0.7) and an inclination that is almost polar with respect to the outer disk.

Price et al. (2018) stated that their results are not strongly sensitive to the companion mass in the range they studied, and a lower planetary mass companion (e.g., $\sim 10\,M_J$) is not clearly excluded. Lacour et al. (2016) and Claudi et al. (2019) showed that both the mass and the orbit of the companion are highly uncertain. For example, Claudi et al. (2019) placed a dynamical constraint on the mass of the companion of $0.26^{+0.16}_{-0.14}\,M_\odot$. Thus, the analysis favors a stellar companion but does not rule out a $10\,M_J$ companion. It is also unclear whether all of the circumstellar disk properties are the result of a single companion. A disk with a very large inner hole, like that of HD 142527, could signal the presence of multiple giant planet companions (Dodson-Robinson & Salyk 2011; Zhu et al. 2011); as in the case of PDS 70bc (Haffert et al. 2019). Thus, the available data allow for the possibility of a planetary mass companion.

The episodic accretion picture can be tested by searching for orbiting companions in their more typical quiescent state with deeper high-contrast imaging than has been performed to date. Orbiting companions may also be identified through submillimeter continuum imaging of circumplanetary disks, IR imaging and spectroscopy of circumplanetary disks, and Gaia astrometry.

ALMA may be able to detect quiescently accreting circumplanetary disks through their dust emission (e.g., Isella et al. 2014; Boehler et al. 2017; Zhu et al. 2018); however, the strength of the emission depends on the extent to which disk solids are filtered out by the gap edge of the outer disk (e.g., Rice et al. 2006) before reaching the circumplanetary disk. Efficient filtering or rapid growth into large solids will reduce the circumplanetary disk optical depth, potentially compromising the detectability of the dust emission signature. Perhaps as a result, circumplanetary disk detections with this approach have been rare to date despite multiple attempts. An exciting possible detection was reported by Pérez et al. (2019) in the HD 100546 system.

Circumplanetary disks can also be detected and studied in the IR. Quiescent circumplanetary disks can potentially be detected through gas emission features from their atmosphere, e.g., with spectroastrometry of 5 μm CO fundamental emission as in HD 100546 (Brittain et al. 2019). Future observations can potentially also distinguish between the stellar versus outbursting circumplanetary disk explanations for the detected companion to HD 142527, e.g., by using IR spectroscopy to measure the gravity of the companion. Compared to the dwarf-like gravity expected for a young low-mass companion,

accretion disks in outburst are expected to show giant-like gravity, e.g., in their 2.3 μm CO overtone absorption (e.g., FU Ori; Kenyon & Hartmann 1995). More sensitive searches for companions to much larger samples of young stars will be possible with imagers on 30 m class telescopes. Zhu (2015) and Szulágyi et al. (2019) suggested that the mid-IR observations will be more sensitive to the presence of forming planets and their circumplanetary disks than the NIR observations pursued thus far.

Longer-wavelength observations are not only better matched to the spectral region where much of the flux is emitted, they are also less sensitive to obscuration by dust in the surrounding protoplanetary disk environment. At first glance, it seems unlikely that extinction by the circumstellar disk is sufficient to account for the low detection rate of forming planets. Simulations of gap opening show that even relatively low-mass planets ($\sim 0.5\,M_J$) in a modest viscosity environment ($\alpha = 10^{-3}$) are able to clear a gap to $\sim 3\%$ of its original density (Fung et al. 2014). For a gap in a transition disk reduced in column density by a roughly a factor of 100–10,000 relative to the minimum mass solar nebula (Furlan et al. 2011; van der Marel et al. 2016), this results in negligible NIR (i.e., K-band) extinction of the forming planet ($\lesssim 0.05$ mag). Once the planet grows to greater than a Jupiter mass, this problem becomes even less severe, so it is plausible that circumstellar disk extinction does not account for the dearth of forming planets imaged in disks. Longer-wavelength observations can test that assumption.

One particularly promising way to identify weakly or nonaccreting gas giant planets in disks is through the use of Gaia astrometry. This method has already been used to measure the mass of the gas giant orbiting the A star β Pic, with a precision of 3 M_J, the stellar reflex motion induced by an 11-13 M_J planet orbiting an A star 20 pc away (Snellen & Brown 2018; Dupuy et al. 2019). A similar approach can be used to measure the mass of the companion to HD 142527 and test our scenario that it is an accreting planet rather than a star. Once the full Gaia time baseline becomes available, along with the expected 100-fold increase in astrometric precision, it should be possible to detect the stellar reflex motion of a sub-Jupiter mass planet ($\gtrsim 0.3\,M_J$) at the distance of HD 142527 (157 pc) or definitively rule out a substellar mass for the companion.

Finally, an observational campaign focused on a larger sample of sources, especially those with dynamical signatures of massive planets (large and deep cavities or two-arm spirals), will constrain the duty cycle and magnitude of outbursts. The fraction of bright circumplanetary disks detected in outburst reflects the duty cycle of the outbursts, which depends on the rate at which the circumplanetary disk grows and empties. As the rate of accretion onto the circumplanetary disk increases, so does the frequency of outbursts, if their magnitude and duration remain the same. If outbursts are more violent than we assume (with planetary accretion rates of $\dot{M}_p \gtrsim 10^{-6}\,M_\odot\,\mathrm{yr}^{-1}$), they will be brighter and the duty cycle lower. Surveys that report upper limits on the luminosity of companions in systems that are expected to harbor gas giant planets are crucial for advancing our understanding of this very important phase of gas giant planet growth.

ORCID iDs

Sean D. Brittain ⓘ https://orcid.org/0000-0001-5638-1330
Ruobing Dong ⓘ https://orcid.org/0000-0001-9290-7846
Zhaohuan Zhu ⓘ https://orcid.org/0000-0003-3616-6822

References

Akiyama, E., Hashimoto, J., Liu, H. B., et al. 2016, AJ, 152, 222
ALMA Partnership, Brogan, C. L., Pérez, L. M., et al. 2015, ApJL, 808, L3
Armitage, P. J., Livio, M., & Pringle, J. E. 2001, MNRAS, 324, 705
Avenhaus, H., Quanz, S. P., Garufi, A., et al. 2018, ApJ, 863, 44
Ayliffe, B. A., & Bate, M. R. 2012, MNRAS, 427, 2597
Baraffe, I., Chabrier, G., Barman, T. S., Allard, F., & Hauschildt, P. H. 2003, A&A, 402, 701
Batygin, K. 2018, AJ, 155, 178
Biller, B., Lacour, S., Juhász, A., et al. 2012, ApJL, 753, L38
Boehler, Y., Weaver, E., Isella, A., et al. 2017, ApJ, 840, 60
Bowler, B. P. 2016, PASP, 128, 102001
Brittain, S. D., Carr, J. S., Najita, J. R., Quanz, S. P., & Meyer, M. R. 2014, ApJ, 791, 136
Brittain, S. D., Najita, J. R., Carr, J. S., et al. 2013, ApJ, 767, 159
Brittain, S. D., Najita, J. R., & Carr, J. S. 2015, Ap&SS, 357, 54
Brittain, S. D., Najita, J. R., & Carr, J. S. 2019, ApJ, 883, 37
Canovas, H., Hardy, A., Zurlo, A., et al. 2017, A&A, 598, A43
Canovas, H., Ménard, F., Hales, A., et al. 2013, A&A, 556, A123
Canovas, H., Montesinos, B., Schreiber, M. R., et al. 2018, A&A, 610, A13
Casassus, S., Hales, A., de Gregorio, I., et al. 2013, A&A, 553, A64
Cassan, A., Kubas, D., Beaulieu, J.-P., et al. 2012, Natur, 481, 167
Christiaens, V., Casassus, S., Absil, O., et al. 2018, A&A, 617, A37
Cieza, L. A., Lacour, S., Schreiber, M. R., et al. 2013, ApJL, 762, L12
Clarke, C. J., Tazzari, M., Juhasz, A., et al. 2018, ApJL, 866, L6
Claudi, R., Maire, A. L., Mesa, D., et al. 2019, A&A, 622, A96
Close, L. M., Follette, K. B., Males, J. R., et al. 2014, ApJL, 781, L30
Cugno, G., Quanz, S. P., Hunziker, S., et al. 2019, A&A, 622, A156
Cumming, A., Butler, R. P., Marcy, G. W., et al. 2008, PASP, 120, 531
Currie, T., Brittain, S., Grady, C. A., Kenyon, S. J., & Muto, T. 2017, RNAAS, 1, 40
Currie, T., Cloutier, R., Brittain, S., et al. 2015, ApJL, 814, L27
Currie, T., Marois, C., Cieza, L., et al. 2019, ApJL, 877, L3
Currie, T., & Sicilia-Aguilar, A. 2011, ApJ, 732, 24
D'Angelo, G., Durisen, R. H., & Lissauer, J. J. 2010, in Giant Planet Formation, ed. S. Seager (Tucson, AZ: Univ. Arizona Press), 319
Dodson-Robinson, S. E., & Salyk, C. 2011, ApJ, 738, 131
Dong, R., & Fung, J. 2017, ApJ, 835, 38
Dong, R., Hall, C., Rice, K., & Chiang, E. 2015a, ApJL, 812, L32
Dong, R., Liu, S.-y., Eisner, J., et al. 2018a, ApJ, 860, 124
Dong, R., Najita, J. R., & Brittain, S. 2018b, ApJ, 862, 103
Dong, R., Zhu, Z., Rafikov, R. R., & Stone, J. M. 2015b, ApJL, 809, L5
Dong, R., Zhu, Z., & Whitney, B. 2015c, ApJ, 809, 93
Dupuy, T. J., Brandt, T. D., Kratter, K. M., & Bowler, B. P. 2019, ApJL, 871, L4
Eisner, J. A. 2015, ApJL, 803, L4
Espaillat, C., Muzerolle, J., Najita, J., et al. 2014, in Protostars and Planets VI, ed. H. Beuther et al. (Tucson, AZ: Univ. Arizona Press)
Fabrycky, D. C., & Murray-Clay, R. A. 2010, ApJ, 710, 1408
Fang, M., van Boekel, R., Wang, W., et al. 2009, A&A, 504, 461
Follette, K. B., Rameau, J., Dong, R., et al. 2017, AJ, 153, 264
Fortney, J. J., Marley, M. S., Saumon, D., & Lodders, K. 2008, ApJ, 683, 1104
Fukagawa, M., Tamura, M., Itoh, Y., et al. 2006, ApJL, 636, L153
Fukagawa, M., Tsukagoshi, T., Momose, M., et al. 2013, PASJ, 65, L14
Fung, J., Artymowicz, P., & Wu, Y. 2015, ApJ, 811, 101
Fung, J., & Dong, R. 2015, ApJL, 815, L21

Fung, J., Shi, J.-M., & Chiang, E. 2014, ApJ, 782, 88
Furlan, E., Luhman, K. L., Espaillat, C., et al. 2011, ApJS, 195, 3
Grady, C. A., Muto, T., Hashimoto, J., et al. 2013, ApJ, 762, 48
Grady, C. A., Polomski, E. F., Henning, T., et al. 2001, AJ, 122, 3396
Gratton, R., Ligi, R., Sissa, E., et al. 2019, A&A, 623, A140
Gregorio-Hetem, J., & Hetem, A. 2002, MNRAS, 336, 197
Gressel, O., Nelson, R. P., Turner, N. J., & Ziegler, U. 2013, ApJ, 779, 59
Guidi, G., Ruane, G., Williams, J. P., et al. 2018, MNRAS, 479, 1505
Haffert, S. Y., Bohn, A. J., de Boer, J., et al. 2019, NatAs, 3, 749
Hall, C., Dong, R., Rice, K., et al. 2019, ApJ, 871, 228
Hall, C., Rice, K., Dipierro, G., et al. 2018, MNRAS, 477, 1004
Hartmann, L., Calvet, N., Gullbring, E., & D'Alessio, P. 1998, ApJ, 495, 385
Hartmann, L., Herczeg, G., & Calvet, N. 2016, ARA&A, 54, 135
Herbig, G. H. 1977, ApJ, 217, 693
Ingleby, L., Calvet, N., Herczeg, G., et al. 2013, ApJ, 767, 112
Isella, A., Benisty, M., Teague, R., et al. 2019, ApJL, 879, L25
Isella, A., Chandler, C. J., Carpenter, J. M., Pérez, L. M., & Ricci, L. 2014,
    ApJ, 788, 129
Jensen, E. L. N., Cohen, D. H., & Gagné, M. 2009, ApJ, 703, 252
Johnson, J. A., Howard, A. W., Bowler, B. P., et al. 2010, PASP, 122, 701
Kenyon, S. J., & Hartmann, L. 1995, ApJS, 101, 117
Kenyon, S. J., Hartmann, L. W., Strom, K. M., & Strom, S. E. 1990, AJ, 99, 869
Keppler, M., Benisty, M., Müller, A., et al. 2018, A&A, 617, A44
Klahr, H., & Kley, W. 2006, A&A, 445, 747
Kratter, K., & Lodato, G. 2016, ARA&A, 54, 271
Kraus, A. L., & Ireland, M. J. 2012, ApJ, 745, 5
Kraus, S., Ireland, M. J., Sitko, M. L., et al. 2013, ApJ, 768, 80
Lacour, S., Biller, B., Cheetham, A., et al. 2016, A&A, 590, A90
Lagrange, A.-M., Gratadour, D., Chauvin, G., et al. 2009, A&A, 493, L21
Ligi, R., Vigan, A., Gratton, R., et al. 2018, MNRAS, 473, 1774
Liskowsky, J. P., Brittain, S. D., Najita, J. R., et al. 2012, ApJ, 760, 153
Long, Z. C., Akiyama, E., Sitko, M., et al. 2018, ApJ, 858, 112
Lubow, S. H., & D'Angelo, G. 2006, ApJ, 641, 526
Lubow, S. H., & Martin, R. G. 2012, ApJL, 749, L37
Lubow, S. H., Seibert, M., & Artymowicz, P. 1999, ApJ, 526, 1001
Luhn, J. K., Bastien, F. A., Wright, J. T., et al. 2019, AJ, 157, 149
Maire, A. L., Stolker, T., Messina, S., et al. 2017, A&A, 601, A134
Malfait, K., Bogaert, E., & Waelkens, C. 1998, A&A, 331, 211
Marino, S., Perez, S., & Casassus, S. 2015, ApJL, 798, L44
Marley, M. S., Fortney, J. J., Hubickyj, O., Bodenheimer, P., & Lissauer, J. J.
    2007, ApJ, 655, 541
Marois, C., Macintosh, B., Barman, T., et al. 2008, Sci, 322, 1348
Martin, R. G., & Lubow, S. H. 2011, ApJL, 740, L6
Mawet, D., Choquet, É., Absil, O., et al. 2017, AJ, 153, 44
Mendigutía, I., Fairlamb, J., Montesinos, B., et al. 2014, ApJ, 790, 21
Mendigutía, I., Oudmaijer, R. D., Schneider, P. C., et al. 2018, A&A, 618, L9

Muto, T., Grady, C. A., Hashimoto, J., et al. 2012, ApJL, 748, L22
Muzerolle, J., Allen, L. E., Megeath, S. T., Hernández, J., & Gutermuth, R. A.
    2010, ApJ, 708, 1107
Nielsen, E. L., De Rosa, R. J., Macintosh, B., et al. 2019, AJ, 158, 13
Pérez, S., Casassus, S., Hales, A., et al. 2019, arXiv:1906.06305
Pineda, J. E., Szulágyi, J., Quanz, S. P., et al. 2019, ApJ, 871, 48
Pontoppidan, K. M., Blake, G. A., & Smette, A. 2011, ApJ, 733, 84
Price, D. J., Cuello, N., Pinte, C., et al. 2018, MNRAS, 477, 1270
Quanz, S. P., Amara, A., Meyer, M. R., et al. 2013, ApJL, 766, L1
Quanz, S. P., Amara, A., Meyer, M. R., et al. 2015, ApJ, 807, 64
Rameau, J., Follette, K. B., Pueyo, L., et al. 2017, AJ, 153, 244
Reggiani, M., Christiaens, V., Absil, O., et al. 2018, A&A, 611, A74
Rice, W. K. M., Armitage, P. J., Wood, K., & Lodato, G. 2006, MNRAS,
    373, 1619
Sallum, S., Follette, K. B., Eisner, J. A., et al. 2015, Natur, 527, 342
Sicilia-Aguilar, A., Hartmann, L. W., Hernández, J., Briceño, C., & Calvet, N.
    2005, AJ, 130, 188
Sissa, E., Gratton, R., Garufi, A., et al. 2018, A&A, 619, A160
Snellen, I. A. G., & Brown, A. G. A. 2018, NatAs, 2, 883
Spiegel, D. S., & Burrows, A. 2012, ApJ, 745, 174
Stone, J. M., Skemer, A. J., Hinz, P. M., et al. 2018, AJ, 156, 286
Szulágyi, J. 2017, ApJ, 842, 103
Szulágyi, J., Dullemond, C. P., Pohl, A., & Quanz, S. P. 2019, MNRAS,
    487, 1248
Szulágyi, J., Masset, F., Lega, E., et al. 2016, MNRAS, 460, 2853
Szulágyi, J., Morbidelli, A., Crida, A., & Masset, F. 2014, ApJ, 782, 65
Szulágyi, J., & Mordasini, C. 2017, MNRAS, 465, L64
Tang, Y.-W., Guilloteau, S., Dutrey, A., et al. 2017, ApJ, 840, 32
Tanigawa, T., Ohtsuki, K., & Machida, M. N. 2012, ApJ, 747, 47
Testi, L., Skemer, A., Henning, T., et al. 2015, ApJL, 812, L38
Thalmann, C., Janson, M., Garufi, A., et al. 2016, ApJL, 828, L17
Uyama, T., Hashimoto, J., Kuzuhara, M., et al. 2017, AJ, 153, 106
van der Marel, N., Verhaar, B. W., van Terwisga, S., et al. 2016, A&A,
    592, A126
Wagner, K., Follete, K. B., Close, L. M., et al. 2018, ApJL, 863, L8
Wagner, K., Stone, J. M., Spalding, E., et al. 2019, ApJ, 882, 20
Wang, J. J., Graham, J. R., Dawson, R., et al. 2018, AJ, 156, 192
Willson, M., Kraus, S., Kluska, J., et al. 2016, A&A, 595, A9
Zhang, K., Bergin, E. A., Blake, G. A., et al. 2016, ApJL, 818, L16
Zhu, Z. 2015, ApJ, 799, 16
Zhu, Z., Andrews, S. M., & Isella, A. 2018, MNRAS, 479, 1850
Zhu, Z., Hartmann, L., & Gammie, C. 2009, ApJ, 694, 1045
Zhu, Z., Ju, W., & Stone, J. M. 2016, ApJ, 832, 193
Zhu, Z., Nelson, R. P., Hartmann, L., Espaillat, C., & Calvet, N. 2011, ApJ,
    729, 47
Zurlo, A., Cugno, G., Montesinos, M., et al. 2020, A&A, 633, A119